Nonideal transport of solute and colloidal tracers through reactive zeolite/iron pellets

Pengfei Zhang

Department of Earth and Atmospheric Sciences, City College of New York, New York, USA

Jirka Šimůnek

Department of Environmental Sciences, University of California, Riverside, Riverside, California, USA

Robert S. Bowman

Department of Earth and Environmental Science, New Mexico Institute of Mining and Technology, Socorro, New Mexico, USA

Received 1 July 2003; revised 14 February 2004; accepted 23 February 2004; published 17 April 2004.

[1] Solute and colloidal tracer tests were conducted in laboratory columns to examine the hydraulic properties of a foamed zeolite/iron pellet material that was developed for in situ remediation of contaminated groundwater. The colloidal tracer (1 μm polystyrene microspheres) moved through the columns much faster than the nonreactive solute tracer tritiated water, reflecting the interpellet preferential flow paths in the packed material. Flow interruption experiments with tritium and bromide showed concentration rebound of both tracers after the interruption (during elution), indicating the existence of nonadvective zones inside the pellets. Inverse modeling of microsphere data using a physical nonequilibrium transport model yielded immobile water content (θ_{im}) equivalent to the intrapellet porosity (0.40), suggesting that the microspheres were excluded from the small intrapellet pores and could only move through the large interpellet pore spaces. Inverse modeling of tritium data using physical nonequilibrium and dual-permeability dual-porosity models yielded θ_{im} values of 0.1–0.2, confirming the existence of nonadvective zones inside the pellets as suggested by the flow interruption experiments. The dual-permeability dual-porosity model also indicated that 6–11% of the total porosity was preferential flow porosity, consistent with the observation of enhanced microsphere transport with respect to tritiated water. Forward modeling with the dual-permeability dual-porosity model suggested that the immobile water in the pellets would not significantly affect the removal efficiency of contaminants subject to sorption and reduction. In contrast, the preferential flow porosity would drastically lower the contaminant removal efficiency. *INDEX TERMS:* 1829 Hydrology: Groundwater hydrology; 1832 Hydrology: Groundwater transport; 1055 Geochemistry: Organic geochemistry; *KEYWORDS:* colloid transport, dual-permeability dual-porosity model, nonideal solute transport, perchloroethylene reduction, preferential flow, zeolite/iron pellets

Citation: Zhang, P., J. Šimůnek, and R. S. Bowman (2004), Nonideal transport of solute and colloidal tracers through reactive zeolite/iron pellets, *Water Resour. Res.*, *40*, W04207, doi:10.1029/2003WR002445.

1. Introduction

[2] Zero-valent iron (ZVI) has been used extensively as a reactive material in subsurface permeable reactive barriers (PRBs) to remove a wide variety of contaminants [*Puls et al.*, 1998; *Reeter et al.*, 1998; *Puls et al.*, 1999a, 1999b; *Vogan et al.*, 1999; *Morrison et al.*, 2001; *Gillham et al.*, 2002; *Kjeldsen and Locht*, 2002]. Since reaction rates are often directly related to the surface area of the ZVI [*Gotpagar et al.*, 1997; *Wang and Zhang*, 1997; *Cao et al.*, 1999; *Ponder et al.*, 2000], fine-grained ZVI with large surface to volume ratio (e.g., ZVI powders) may be used to enhance reaction rates and contaminant removal efficiencies. However, the use of fine-grained ZVI (or any fine-grained reactive materials) will reduce the hydraulic conductivity of PRBs [*Grant et al.*, 1987], diminishing the ability of the PRBs to effectively capture contaminant plumes. Therefore efforts have been made to increase the hydraulic conductivity of ZVI PRBs by mixing granular ZVI with coarse sand [*O'Hannesin and Gillham*, 1998; *Puls et al.*, 1999b] or by making foamed aluminosilicate-bound ZVI pellets [*Naftz et al.*, 2000]. Recently, a reactive pellet material was developed by coating surfactant-modified zeolite (SMZ) and ZVI powders onto a highly porous glass foam substrate [*Zhang et al.*, 2002]. This novel process allowed the use of fine-grained reactive materials to produce pellets with high reactivity, strong mechanical strength, and superior hydraulic conductivity (9.7 cm s^{-1}) [*Zhang et al.*, 2002]. The ~10 cm s^{-1} hydraulic conductivity is 2–3 orders of magnitude greater

0043-1397/04/2003WR002445$09.00

Table 1. Particle Size Distribution of Zeolite and Zero-Valent Iron (ZVI) Powders Used to Manufacture the Reactive Zeolite/ZVI Pellets

Zeolite			ZVI		
Sieve Range	Size Range, μm	Zeolite Retained, %	Sieve Range	Size Range, μm	ZVI Retained, %
40–70	212–425	30.4	70–78	177–212	7
70–100	150–212	14.6	80–100	150–177	14
100–140	102–150	14.5	100–120	125–150	20
140–200	74–102	7.7	120–200	74–125	37
200–350	42–74	8.4	>200	<74	22
>350	<42	23.7			
Total		99.3	Total		100

than that of granular ZVI, granular ZVI mixed with coarse sand, or foamed aluminosilicate-bound ZVI pellets [*O'Hannesin and Gillham*, 1998; *Puls et al.*, 1999a, 1999b; *Naftz et al.*, 2000]. While highly permeable, SMZ/ZVI pellets (2.5-cm cubes), and other pelletized reactive materials, have some potential drawbacks: (1) Preferential flow paths may exist between the pellets due to their large sizes; and (2) nonadvective zones may be present within pellet coatings (e.g, the fine-grained SMZ and ZVI powders used here). The presence of preferential flow paths and nonadvective zones may limit the mass transfer of contaminants to the reactive sites of pellets, leading to decreased contaminant removal efficiencies. Understanding the hydraulic properties of the SMZ/ZVI pellets can lead to optimized production processes for these and other composites, and to improved modeling of reactive solute transport through PRBs formed of pelletized materials.

[3] Colloidal-sized particles have been observed to travel faster than dissolved solutes in porous media containing macropores or fractures (preferential flow paths) [*Champ and Shroeter*, 1988; *Harvey et al.*, 1989; *McKay et al.*, 1993; *Vilks and Bachinski*, 1996; *Grolimund et al.*, 1998; *Pang et al.*, 1998; *Deborde et al.*, 1999; *Zhang et al.*, 2001a; *Scheibe and Wood*, 2003]. The enhanced transport of colloids is often attributed to exclusion processes. Because of their large sizes, colloids are prevented from entering some convective pores of the same scale as the colloids and are rerouted to the macropores or fractures (a process known as macroscopic "pore exclusion" [*Ginn*, 2002]). Since velocity is greater in the macropores or fractures, colloids travel faster on average than nonreactive solutes. Therefore comparison of breakthrough curves (BTCs) of colloidal particles versus BTCs of a nonreactive solute tracer can indicate the presence or absence of preferential flow paths. Enhanced transport of colloidal particles may also arise from microscopic (pore-scale) exclusion processes. For example, within a pore throat, colloids are prevented from approaching pore walls due to repulsive interaction forces (charge exclusion) and/or large colloid sizes (chromatographic effect). Since colloids do not experience the low velocities near the pore walls, the mean velocity of colloids is increased relative to nonreactive solute tracers. While microscopic exclusion processes are important in coarse-grained media where the colloids are far smaller than almost all pores [*Harter et al.*, 2000], macroscopic "pore exclusion" plays a significant role in media containing aggregates and preferential flow paths for enhanced colloid transport.

[4] Flow interruption during the transport of a nonreactive solute is a sensitive means of determining the presence of physical nonequilibrium, or diffusive mass transfer between mobile (e.g., macropores or fractures) and immobile (e.g., fine matrix) zones [*Brusseau et al.*, 1989; *Hu and Brusseau*, 1995; *Reedy et al.*, 1996; *Brusseau et al.*, 1997]. During tracer injection (i.e., on the ascending limb of a BTC), solute concentrations within macropores or fractures are greater than those within the fine matrix. During flow interruption the solute diffuses from the macropores or fractures into the fine matrix, resulting in a decrease in effluent concentration after the flow interruption [*Hu and Brusseau*, 1995; *Reedy et al.*, 1996]. Conversely, during tracer elution (i.e., on the descending limb of a BTC), solute concentrations within the macropores or fractures are lower than those within the fine matrix. During flow interruption the solute diffuses back from the fine matrix to the macropores or fractures, leading to an increase in effluent concentration after the flow interruption [*Reedy et al.*, 1996; *Brusseau et al.*, 1997]. Therefore, for a nonreactive tracer, a concentration perturbation upon imposition of flow interruption is indicative of the presence of physical nonequilibrium, or nonadvective zones.

[5] The objectives of this study were to (1) verify the existence of preferential flow paths and nonadvective zones in the packed reactive zeolite/ZVI pellets; (2) quantify the fraction of preferential flow porosity and immobile water content; and (3) determine the impacts of preferential flow paths and nonadvective zones on contaminant reduction. Transport experiments with a colloidal tracer (1 μm polystyrene microspheres) and a nonreactive tracer (tritiated water) were carried out to determine the presence of preferential flow paths in the packed pellets. Flow interruption experiments with the tritiated water and bromide were conducted to determine the presence of nonadvective zones inside the pellets. Microsphere and tritium breakthrough data were inversely modeled using physical nonequilibrium and dual-permeability dual-porosity transport models to further quantify the fraction of preferential flow porosity and immobile water content. Forward modeling using the dual-permeability dual-porosity model was carried out to determine the effects of variable preferential flow porosity and immobile water content on the reduction of contaminants subject to sorption and reduction.

2. Materials and Methods

2.1. Pellet Preparation

[6] The pellet-production process involved coating zeolite powder (St. Cloud Mine, Winston, New Mexico) and ZVI powder (Peerless Metal Powders and Abrasives, Detroit, Michigan) onto a highly porous glass foam substrate (Cercona of America, Inc., Dayton, Ohio). The particle size distribution of the zeolite and ZVI powders is presented in Table 1. Foam slabs 22.9 cm square and 2.5 cm thick were slotted (2.5-cm slots, 1.25 cm deep, running perpendicular to one another on opposite sides of the slab) for easy breaking into 2.5-cm cubes following coating with zeolite and ZVI. To coat the glass foam substrate, a homogeneous slurry of zeolite powder (14.5% by weight),

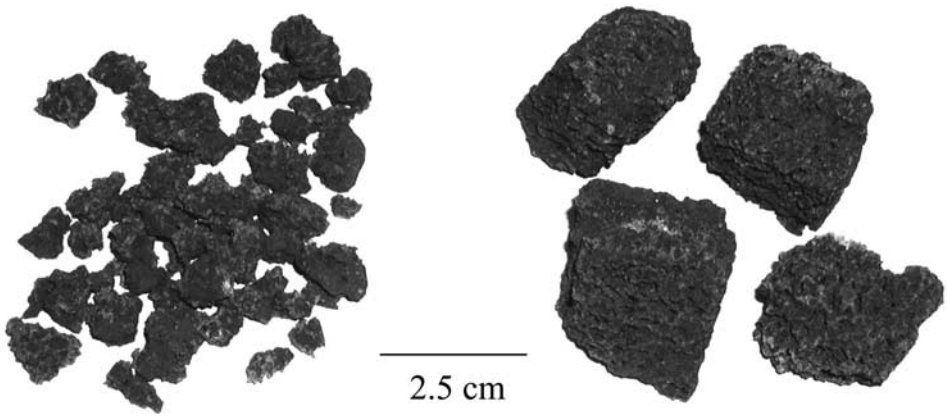

Figure 1. Crushed zeolite/zero-valent iron (ZVI) pellets and original 2.5-cm cubes.

ZVI powder (43.5% by weight), and water (42.0% by weight) was prepared in a large mixing bath. The foam slabs were dipped into the slurry for about 5 s, removed from the bath, and dried at room temperature for 4 days. The dipping process allowed the slurry to flow into the foam substrate without significant clogging of the pore structure [*Bowman et al.*, 2002]. When dry, the zeolite/iron mixture adhered tightly to the silica foam substrate. The dried slabs were then broken into 2.5-cm cubes (Figure 1) for a pilot-scale PRB test [*Bowman et al.*, 2002]. For laboratory column experiments, zeolite/ZVI cubes were further crushed to smaller size pellets (0.5–1.0 cm in one dimension, Figure 1) using a hammer and a screwdriver. During the crushing process, about 50% of the zeolite/ZVI coating was lost, making the final composition of the crushed pellets approximately 12.5% zeolite, 37.5% iron, and 50% silica foam substrate by weight. Readers are referred to *Bowman et al.* [2002] and *Zhang et al.* [2002] for more details of the preparation of the reactive zeolite/ZVI pellets, and the performance of the pellets for chemically reducing perchloroethylene (PCE) and chromate in bench- and pilot-scale tests.

2.2. Transport Experiments

[7] Four CHROMAFLEX™ glass chromatograph columns (Kontes, Vineland, New Jersey), 30 cm long by 4.8-cm diameter, were packed with the crushed zeolite/ZVI pellets. The columns were purged with CO_2 for 1.5 hours to promote water saturation, then fed with degassed synthetic groundwater (0.52 mM $NaHCO_3$, 0.08 mM $MgSO_4$, 0.09 mM $CaCl_2$, 0.01 mM KNO_3, 0.12 mM $CaCO_3$, and 0.02 mM $Mg(NO_3)_2$) at a linear velocity of 0.5 m d^{-1}. This synthetic groundwater was used as the aqueous matrix for all subsequent experiments. The 0.5 m d^{-1} velocity used here is typical of groundwater velocities and was identical to the groundwater velocity in the pilot-scale PRB filled with the reactive zeolite/ZVI pellets [*Bowman et al.*, 2002]. All injections were conducted in an upward flow mode with a PHD 2000 programmable multichannel syringe pump (Harvard Apparatus, Holliston, Massachusetts). The syringe pump was used in order to (1) minimize pulses in flow; (2) eliminate the crushing of soft colloids (e.g., polystyrene microspheres) by the squeezing motion of peristaltic pumps; (3) avoid soft tubing (e.g., silicone, Tygon®, or Viton® tubing often required in peristaltic pumps) that would react with organic solvents (e.g., PCE) and interfere with our subsequent study of reductive dechlorination of PCE by the reactive pellets; and (4) avoid changes in flow rate due to stretching of the soft tubing over time. The weight of each column was determined approximately every pore volume (PV) until there was no weight difference between two consecutive measurements. At that time a column was considered fully saturated and the porosity of the packed pellets was determined by the difference between the saturated weight and the dry weight of the column. The bulk density of the packed pellets was calculated based on the dry mass of the packed pellets and the volume of the column.

[8] Upon saturation, two columns were modified with the cationic surfactant hexadecyltrimethylammonium chloride (Aldrich Chemical Company, Milwaukee, Wisconsin) for the purpose of enhancing contaminant removal [*Bowman et al.*, 2002; *Zhang et al.*, 2002]. The surfactant modification was not expected to change the physical properties (e.g., porosity and hydraulic conductivity) of the pellets [*Zhang et al.*, 2002], but was expected to alter the surface chemistry of the pellets by reversing zeolite's surface charge from net negative to net positive via a two-step process: (1) the formation of a surfactant monolayer with positively charged surfactant head groups adsorbed on the surface (via electrostatic interactions) and the hydrophobic tails orientated toward solution; and (2) the formation of a second surfactant layer (via hydrophobic interactions among the surfactant tails) with the positively charged surfactant head groups orientated toward solution [*Li and Bowman*, 1998]. As a result, anions such as bromide (a solute commonly considered as a nonreactive tracer) would be adsorbed [*Li and Bowman*, 1997] and retarded during transport through the surfactant-modified pellets.

[9] A 3-PV pulse of tritiated water (11,800 counts min^{-1} mL^{-1}) was injected into the columns together with KBr (100 mg L^{-1} as Br^-) at a linear velocity of 0.5 m d^{-1}, followed by 7 PV of tracer-free synthetic groundwater. Flow rates were verified from the cumulative volume of effluent over time. Effluent samples were collected in glass scintillation vials using Retriever II fraction collectors (ISCO Inc., Lincoln, Nebraska). Flow was stopped at the second PV (during tracer injection) and fourth PV (during tracer

Table 2. Properties of the Packed Columns and Conditions of the Transport Experiments

				v, m d^{-1}		Input Pulse (PV)	
Column	Length, cm	θ	ρ_b, g cm^{-3}	Solute	Colloid	Solute	Colloid
1	30.0	0.813	0.666	0.482	0.479	2.96	2.95
2	30.0	0.810	0.668	0.492	0.489	2.96	2.97
3	30.0	0.808	0.663	0.501	0.502	3.01	3.04
4	30.0	0.814	0.670	0.500	0.505	3.03	3.07

elution) of the experiment for 29 hours (2 PV) each time to allow possible diffusive mass transfer of solutes into or out of nonadvective domains in the packed pellets. A separate transport experiment with carboxylate-modified polystyrene microspheres (1.0 μm diameter, 5.0×10^6 spheres mL^{-1}, Molecular Probes, Eugene, Oregon) was also conducted in a similar manner (i.e., 3-PV pulse of injection followed by 7 PV of elution, at a linear velocity of 0.5 m d^{-1}) except that there was no flow interruption. The microsphere transport experiment was separated from the solute tracer test to avoid radioactive tritium contamination of the flow cytometer used for microsphere analysis. The properties of the packed columns and conditions of the transport experiments are summarized in Table 2.

2.3. Methods of Analysis

[10] Tritium was analyzed by liquid scintillation counting (Beckman LS 6500, Palo Alto, California) after mixing 1 mL of effluent sample with 5 mL of Ecolite$^+$ scintillation cocktail (ICN Biomedical, Costa Mesa, California). Br^- concentrations were measured using an ion specific electrode (Orion, Beverly, Massachusetts) and a model Φ 45 pH meter (Beckman Instruments, Inc., Fullerton, California), after adjusting the ionic strength of the effluent sample with ionic strength adjustor (Orion). The electrode was calibrated daily using Br^- standard solutions (Orion).

[11] The microsphere concentrations were determined using flow cytometry (FACScan Analyzer, Becton Dickenson Immunocytometry Systems, San Jose, California). The flow cytometry method is easy and fast (30–40 samples h^{-1}), and has been used by many researchers for enumerating bacterial cells and microspheres [*Stewart and Steinkamp*, 1982; *Molema et al.*, 1998; *Fuller et al.*, 2000; *DeFlaun et al.*, 2001]. The yellow-green fluorescent microspheres were excited with an argon laser at a wavelength of 488 nm, and the emitted fluorescence was detected at 515–545 nm. Three milliliters of effluent sample was transferred to a polystyrene tube and sonicated for about 30 s to disperse any coagulated colloids prior to analysis. Samples were withdrawn by the flow cytometer at ~12 μL min^{-1} and the cumulative counts over 1 min were recorded. Solutions with known concentrations of the microspheres (5.0×10^2 up to 5.0×10^6 spheres mL^{-1}) were analyzed daily to prepare calibration curves for converting raw counts to microsphere concentrations in spheres per milliliter. The detection limit for this method was about 5.0×10^2 spheres mL^{-1}, and the linear response range was between 5.0×10^2 and 5.0×10^6 spheres mL^{-1}.

[12] Hydraulic conductivity of the pellets was measured using a constant head method [*Freeze and Cherry*, 1979]. Sixteen well-shaped cubes were used to estimate the internal porosity (intrapellet porosity). The internal porosity of the pellets was determined as the difference between the total cube volume (calculated from the dimensions) and the volume of solids (determined from the volume of water displaced by the cubes after saturation). It was assumed that the internal porosity did not change significantly during the crushing process.

2.4. Transport Modeling

[13] The packed reactive zeolite/ZVI pellets have large interpellet pore spaces (up to several millimeters in dimension), small intrapellet pores (5–20 μm), and possible nonadvective zones within the coating (due to the fine size of the zeolite/ZVI powders). Therefore a dual-permeability dual-porosity conceptual model modified from *Šimůnek et al.* [2003] was used to describe the movement of water and solutes in the packed pellets. This model assumes that the porous medium consists of two interacting domains: a mobile fracture domain, and a matrix domain containing both mobile and immobile regions. For reactive solute transport, the flow equations for the fracture (subscript f), the mobile region of the matrix (subscript m), and the immobile region of the matrix (subscript im) are as follows, respectively:

$$\frac{\partial(\theta_f + f\rho_b K_d)C_f}{\partial t} = \frac{\partial}{\partial x}\left(\theta_f D_f \frac{\partial C_f}{\partial x}\right) - \frac{\partial q_f C_f}{\partial x} - \frac{\Gamma_s}{w} - f\rho_b K_d \mu_s C_f \tag{1}$$

$$\frac{\partial[\theta_m + (1-f)e\rho_b K_d]C_m}{\partial t} = \frac{\partial}{\partial x}\left(\theta_m D_m \frac{\partial C_m}{\partial x}\right) - \frac{\partial q_m C_m}{\partial x} + \frac{\Gamma_s}{1-w} - \omega(C_m - C_{im}) - (1-f)e\rho_b K_d \mu_s C_m \tag{2}$$

$$\frac{\partial[\theta_{im} + (1-f)(1-e)\rho_b K_d]C_{im}}{\partial t} = \omega(C_m - C_{im}) - (1-f)(1-e)\rho_b K_d \mu_s C_{im} \tag{3}$$

where t is time, x is the travel distance, ρ_b is the bulk density, K_d is the sorption constant, μ_s is the solid phase first-order decay constant, θ_f is the fracture (preferential flow) porosity, θ_m is the porosity in mobile regions of the matrix, θ_{im} is the porosity in immobile regions of the matrix, D_f is the dispersion coefficient in the fractures, D_m is the dispersion coefficient in mobile regions of the matrix, C_f is the solute concentration in the fractures, C_m is the solute concentration in mobile regions of the matrix, C_{im} is the solute concentration in immobile regions of the matrix, q_f is the flux in the fractures, q_m is the flux in mobile regions of the matrix, w is the ratio of the fracture domain to total soil volume (equal to the ratio of fracture porosity θ_f and total porosity θ when porosity in each overlapping region is assumed to be the same), ω is the mass transfer coefficient between mobile and immobile water in the matrix, Γ_s is the solute mass transfer rate between the fractures and the mobile water in the matrix, f is the fraction of sorption sites associated with the fractures, $(1 - f)$ is the fraction of sorption sites associated with the matrix, e is the fraction of sorption sites associated with mobile water in the matrix, and $(1 - e)$ is the fraction of sorption sites associated with

Table 3. Parameters for Optimization During Inverse Modeling With Various Transport Models

Tracer	Conceptual Model	Optimized Parameter
Microspheres	equilibrium	α_L, k_a, k_d
	nonequilibrium	α_L, θ_{im}, k_a, k_d
Tritium in all columns, Br^- in columns 1 and 2	nonequilibrium dual-permeability dual-porosity	α_L, θ_{im}, ω q_m, w, θ_{im}, α_s, ω, $\alpha_{L,f}$
Br^- in columns 3 and 4	nonequilibrium	θ_{im}, ω, K_d

immobile water in the matrix. This model assumes that the reduction of contaminants only occurs on the surface of reactive materials and the reduction rate coefficient is the same for all domains. The dispersion coefficient for a specific domain (D_f or D_m) is expressed as the product of dispersivity ($\alpha_{L,f}$ or $\alpha_{L,m}$) and pore water velocity in that domain. The solute mass transfer rate Γ_s is expressed as [*Gerke and van Genuchten*, 1996]

$$\Gamma_s = \alpha_s(1-w)\left(C_f - C_m\right) \tag{4}$$

where α_s is the first-order solute mass transfer coefficient between the fracture and the mobile water in the matrix, expressed as

$$\alpha_s = \frac{\beta}{d^2} D_a \tag{5}$$

where β is the shape factor (15 for spheres), d is the effective "diffusion" path length (half the aggregate width or half the fracture spacing), and D_a is the effective diffusion coefficient representing the diffusion properties of the fracture-matrix interface as well as other parameters [*Gerke and van Genuchten*, 1996].

[14] If the fracture porosity (θ_f) is zero, then the dual-permeability dual-porosity model is reduced to a dual-porosity model (also called physical nonequilibrium model, or mobile-immobile (MIM) model). If the immobile water content (θ_{im}) is zero, the dual-porosity model is further reduced to the so-called equilibrium model. For nonreactive solute tracers the reduction rate coefficient (μ_s) and the sorption constant (K_d) are zero, and the terms associated with these parameters can be omitted.

[15] Colloidal particles undergo attachment and detachment during transport through porous media [*Harvey and Garabedian*, 1991; *Hornberger et al.*, 1992; *McCaulou et al.*, 1994; *Ryan and Elimelech*, 1996; *Hendry et al.*, 1997, 1999; *Zhang et al.*, 2001b]. In addition, colloids are excluded from some small pores due to the large sizes and low diffusion constants of the colloids. A physical nonequilibrium conceptual model (MIM model) was used to describe the transport of the microspheres through the packed reactive zeolite/ZVI pellets. This model divides the porous medium into two regions (as opposed to the three regions in the solute transport model): a mobile region (accessible to the microspheres), and an immobile region (inaccessible to the microspheres due to macroscopic "pore exclusion"). This model accounts for colloid attachment and detachment and assumes that there is no mass transfer between mobile and immobile zones (i.e., the microspheres are completely excluded from the immobile zones). The governing equations are as follows:

$$\frac{\partial C}{\partial t} + \frac{\rho_b}{\theta_m}\frac{\partial S}{\partial t} = D\frac{\partial^2 C}{\partial x^2} - v\frac{\partial C}{\partial x} \tag{6}$$

$$\frac{\rho_b}{\theta_m}\frac{\partial S}{\partial t} = k_a C - k_d \frac{\rho_b}{\theta_m} S \tag{7}$$

where C is the colloid concentration in aqueous phase, S is the colloid concentration on solid phase, D is the dispersion coefficient, v is the pore water velocity, k_a is the colloid attachment rate coefficient, k_d is the detachment rate coefficient, and θ_m is the "mobile" water content, or to be more accurate, the porosity accessible to colloids. The physical nonequilibrium model is reduced to the equilibrium model if θ_m is replaced by the total porosity.

[16] The modified HYDRUS-1D computer code [*Šimůnek et al.*, 1998] was used to implement the transport models described above. In HYDRUS-1D, parameter optimization is achieved by using the Levenberg-Marquardt nonlinear optimization method (a weighted least squares approach) [*Šimůnek et al.*, 1998]. The parameters for optimization in various transport models are summarized in Table 3. Since dispersivity (α_L) covaries with sorption constant (K_d), the α_L values for bromide in columns 3 and 4 (subject to adsorption) were fixed in the nonequilibrium model, using the α_L values derived from tritium data of these columns. For the dual-permeability dual-porosity model the effective "diffusion" path length (d) was set to 0.4 cm (half the pellet size), and the dispersivity in mobile regions of the matrix ($\alpha_{L,m}$) was fixed at 1.0 cm, a value appropriate for columns packed with unconsolidated geological materials [*Freeze and Cherry*, 1979]. Inverse modeling with the dual-permeability dual-porosity model was not attempted for bromide data from columns 3 and 4, since fractions of adsorption sites associated with different domains could not be independently determined. Multiple inverse simulations with different initial parameter estimates were carried out to ensure the uniqueness of optimized parameter values. Flow interruption was implemented in HYDRUS-1D by changing the boundary conditions from finite flux to zero flux. In addition to optimized parameter values, HYDRUS-1D also provided statistical information such as the 95% confidence interval for each fitted parameter and the goodness of fit (r^2) of the simulations to the observed data [*Šimůnek et al.*, 1998].

[17] Forward modeling using the dual-permeability dual-porosity model with various fractions of preferential flow porosity (w) and immobile water contents (θ_{im}) was carried out to examine the effects of w and θ_{im} on contaminant reduction. The sorption constant (K_d = 1.0 L kg^{-1}) and reduction rate coefficient (μ_s = 0.5 h^{-1}) used in the model are those appropriate for PCE sorption/reduction by the SMZ/ZVI pellets [*Zhang et al.*, 2002]; other transport parameter values (L = 30 cm, θ = 0.81, ρ_b = 0.67 g cm^{-3}, d = 0.4 cm, v = 0.5 m h^{-1}, $\alpha_{L,m}$ = 1 cm, $\alpha_{L,f}$ = 5 cm, $\alpha_s = 2.4 \times 10^{-4}$ h^{-1}, and $\omega = 3.7 \times 10^{-3}$ h^{-1}) were determined for this study (see section 3). It is assumed

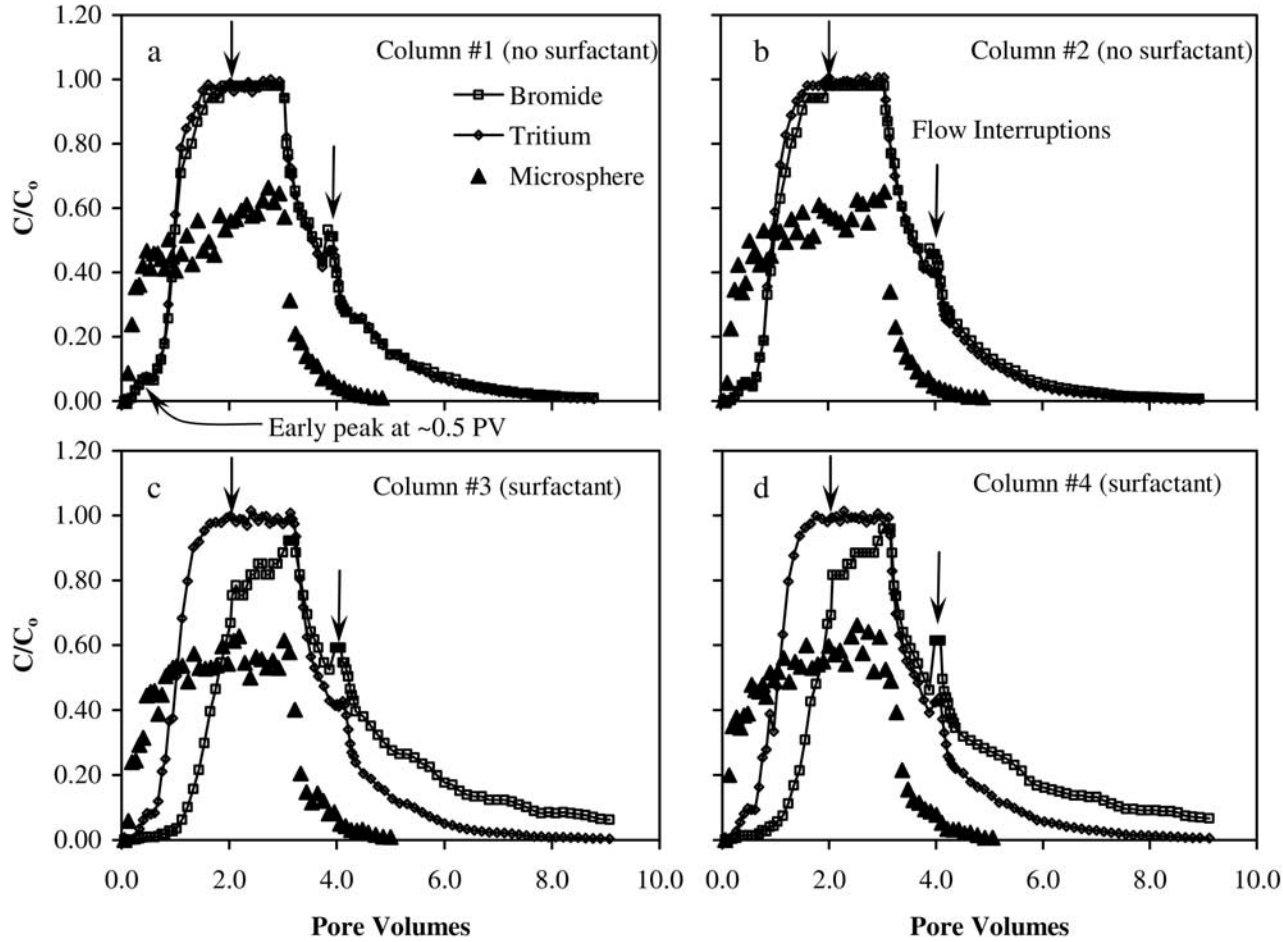

Figure 2. Breakthrough curves for the bromide, tritium, and microsphere tracers. The microspheres broke through the columns much faster than the nonreactive solute tracers. Bromide was retarded with respect to the tritium tracer in the surfactant-treated columns 3 and 4. Flow interruptions occurred at the 2 and 4 pore volume (PV) (indicated by the arrows) for the solute tracers. A solute concentration rebound was evident following the 4-PV interruption.

that every 1% of the preferential flow porosity carries 2.9% of the total flux (see discussion in section 3.5.2) but only contains 0.1% of the total reactive sites (i.e., reactive sites are mainly associated with the matrix porosity). It is further assumed that the reactive sites in the matrix are evenly distributed between the mobile and immobile regions. A constant concentration solute input was used for each simulation, and the effluent C/C_o (relative concentration) at steady state (or plateau of a BTC) was plotted against w or θ_{im}.

3. Results and Discussion

3.1. Pellet Properties

[18] The columns packed with the crushed pellets had a very high porosity (0.81) and a very low bulk density (0.66–0.67 g cm^{-3}; Table 2). The internal porosity (intra-pellet porosity) of the pellets was 0.40, approximately 50% of the total porosity. The hydraulic conductivity of the crushed pellets was 9.7 cm s^{-1}; the original larger pellets (2.5-cm cubes) would have an even higher hydraulic conductivity. The pellets also showed excellent mechanical strength, with no physical deterioration evident after months of operation in a pilot-scale PRB [*Bowman et al.*, 2002].

3.2. Breakthrough Curves

[19] All tritium BTCs exhibited asymmetric shapes with early breakthrough and extended tailing (Figure 2), indicating nonideal transport [*Hu and Brusseau*, 1995]. Close examination of the tritium BTCs revealed a small peak or shoulder at about 0.5 PV prior to full breakthrough (Figure 2). A similar early peak was observed when nitrate was transported through a silica sand column with a simulated fracture in the center; the peak was attributed to the rapid transport of a small fraction of the nitrate through the fracture [*Li and Ghodrati*, 1997]. Therefore the small early peak observed in our study may indicate the presence of preferential flow in the column packed with the reactive zeolite/ZVI pellets.

[20] Bromide BTCs from columns 1 and 2 (without surfactant modification) were almost identical to the tritium BTCs from those columns (Figures 2a and 2b). For these columns no adsorption of bromide occurred and the bromide tracer behaved similar to the nonreactive tritium tracer. Bromide in columns 3 and 4 (with surfactant modification), however, was significantly retarded with respect to the

Table 4. Percent Mass Recovery of the Solute and Colloidal Tracers After Transport Through the Columns Packed With the Reactive Zeolite/ZVI Pellets

Column	Tritium	Bromide	Microsphere
1, no surfactant	101.2	100.2	55.9
2, no surfactant	99.5	98.8	57.4
3, surfactant	101.2	92.8	56.2
4, surfactant	98.9	91.2	57.9

tritium tracer (Figures 2c and 2d). The surfactant-modified pellets are expected to possess positive surface charges and reversibly adsorb Br^- [*Li and Bowman*, 1997], leading to the retardation of the bromide tracer.

[21] The microspheres appeared in the effluent much earlier than the nonreactive tritium tracer in all four columns, and the BTCs also exhibited asymmetric shapes and extended tailing (Figure 2). As mentioned in section 1, colloidal particles are restricted to fractures and macropores due to their large sizes, and travel faster on average than solute tracers in porous media containing preferential flow paths. Therefore the earlier breakthrough of the microspheres with respect to tritium is indicative of the presence of preferential flow paths, consistent with the observation of the early tritium peak.

3.3. Flow Interruption

[22] The flow interruption during tracer elution (at 4 PV) resulted in concentration rebound for both the tritium and bromide tracers in all columns (Figure 2). The concentration rebound of the nonreactive tracers (i.e., tritium in all columns and Br^- in columns 1 and 2) is a clear indication of diffusive mass transfer of the tracers between advective zones and immobile zones in the pellets [*Reedy et al.*, 1996; *Brusseau et al.*, 1997]. The immobile zones likely existed within the coating, due to the fine size of the zeolite and ZVI powders used (Table 1). In contrast to the flow interruption at 4 PV, the flow interruption at 2 PV (during tracer injection) did not cause a noticeable concentration decrease (Figure 2). At 2 PV, the tritium concentration (in all four columns) and the bromide concentration (in columns 1 and 2) were almost 100% of the input concentration (Figure 2), and the lack of effluent concentration change implies near-equilibrium conditions [*Brusseau et al.*, 1989].

3.4. Mass Recovery

[23] Solute and colloid mass recoveries for the four columns (determined by trapezoidal integration of the areas under the BTCs) are shown in Table 4. Full mass recovery was achieved for the tritium tracer in all four columns, and for the bromide tracer in Columns 1 and 2 (Table 4). The 91–93% mass recovery of bromide in columns 3 and 4 (Table 4) was due to termination of the experiments prior to full bromide elution, when the effluent bromide concentrations were still around 6% of the input concentration (Figures 2c and 2d). The 56–58% mass recovery of microspheres (Table 4) was due to the irreversible attachment of a fraction of the microspheres onto the pellets.

3.5. Inverse Modeling Results

[24] Inverse modeling of the microsphere data yielded the same unique values of optimized parameters for both the equilibrium and the nonequilibrium models. However, for the solute tracers, simulations with the physical nonequilibrium model converged to three different solutions with either (1) an extremely small immobile water content ($\theta_{im} \approx 0$), (2) a very large θ_{im} value (close to the total porosity of 0.8) with a large mass transfer coefficient, or (3) a θ_{im} value around 0.15. The first two solutions are essentially the equilibrium solutions, and our system was clearly not an equilibrium one (see discussion in sections 3.2 and 3.3). The third solution reflects the properties of the pellets and will be discussed further in section 3.5.2. Inverse modeling of the solute data with the dual-permeability dual-porosity model yielded unique values for five (q_m, w, θ_{im}, α_s, and ω) out of the six parameters optimized. The sixth parameter ($\alpha_{L,f}$) varied significantly, and some intermediate values will be presented in section 3.5.2.

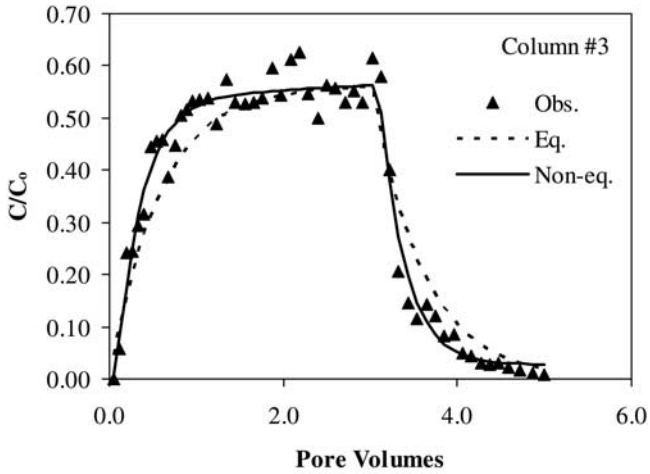

Figure 3. Best fit simulations of the microsphere data (column 3) using the equilibrium and physical nonequilibrium models. The nonequilibrium model provided a significantly improved fit.

3.5.1. Colloidal Tracer

[25] The equilibrium model gave reasonable fits to the observed microsphere BTCs (see an example of column 3 data in Figure 3), but yielded extremely high dispersivity values (average 1.3×10^3 cm, or 43 times the length of the column; data not shown). The unrealistically high dispersivity values imply that the equilibrium model attempts to lump all processes unaccounted for in the conceptual model into the dispersivity. Therefore the equilibrium model is not adequate in describing the transport of microspheres through the packed zeolite/ZVI pellets. The physical non-

Table 5. Optimized Parameter Values for the Microspheres Using the Physical Nonequilibrium Model[a]

Column	α_L, cm	θ_{im}	k_a, h^{-1}	k_d, h^{-1}	r^2
1	29 ± 38	0.45 ± 0.10	0.13 ± 0.04	0.003 ± 0.001	0.96
2	25 ± 25	0.40 ± 0.10	0.10 ± 0.03	0.002 ± 0.002	0.96
3	29 ± 24	0.35 ± 0.08	0.10 ± 0.03	0.002 ± 0.001	0.97
4	30 ± 32	0.40 ± 0.10	0.11 ± 0.03	0.002 ± 0.002	0.96
Average	28	0.40	0.11	0.002	

[a]The 95% confidence limits are indicated by the number following the plus/minus sign.

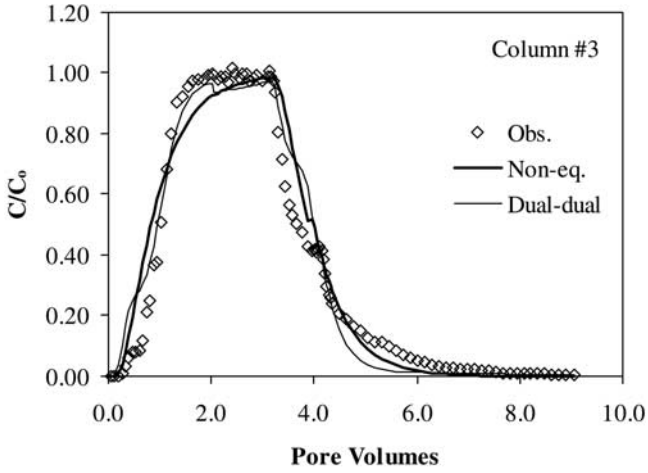

Figure 4. Best fit simulations of the tritium data (column 3) using the nonequilibrium and dual-permeability dual-porosity models. The dual-permeability dual-porosity model fit the ascending limb and plateau of the breakthrough curve (BTC) better than the nonequilibrium model but fit the descending limb and tail less satisfactorily.

equilibrium model significantly improved the fit (Figure 3) and yielded much lower dispersivity values (average 28 cm, Table 5). Furthermore, the physical nonequilibrium model gave θ_{im} (porosity inaccessible to the microspheres) values similar to the independently measured intrapellet porosity of 0.40 (Table 5), indicating that the microspheres were excluded from the intrapellet pores and could only transport through the large interpellet pore spaces. This exclusion of microspheres from the intrapellet pores was further supported by the fact that the microspheres transported through the packed pellets identically despite the difference in pellet surface chemistry (see microsphere BTCs in Figures 2a–2d). Surfactant-modification of the zeolite/ZVI pellets (columns 3 and 4) reversed the surface charge of the pellets from net negative to net positive [*Li and Bowman*, 1998], as reflected in the bromide retardation in these columns. The charge reversal should also have resulted in significant electrostatic attractions for the microspheres (slightly negative) at close range. The lack of increased microsphere removal with the surfactant-modified pellets (columns 3 and 4) suggested that the majority of the microspheres were not in close contact with the pellet surfaces, consistent with the characteristics of transport through large interpellet pore spaces. The removal of a fraction (42–44%) of the microspheres was likely due to the capture of the microspheres by external asperities of the pellets (Figure 1). The apparent velocity of the microspheres was about 1.6 times the apparent velocity of the conservative tritium tracer, based on the physical nonequilibrium model.

3.5.2. Solute Tracers

[26] The simulated BTCs using the physical nonequilibrium model showed good agreement with the observed solute BTCs (see an example of column 3 tritium data in Figure 4). The immobile water content (θ_{im}) derived from the nonequilibrium model varied from 0.14 to 0.19 with an average of 0.15 (Table 6). These θ_{im} values implied that 35–48% of the intrapellet porosity contained immobile water, confirming the presence of nonadvective zones inside the pellets as indicated by the flow interruption experiments. The mass transfer coefficients varied from 0.06 to 0.15 h^{-1} (Table 6), within the range observed (using similar MIM models) for tritium and bromide in synthetic aggregated porous media [*Hu and Brusseau*, 1995] and field soils [*Reedy et al.*, 1996; *Casey et al.*, 1997].

[27] Conceptually, the dual-permeability dual-porosity model describes the hydraulic properties of the packed pellets better than the physical nonequilibrium model (see section 2.4). However, the more complex dual-permeability dual-porosity model only improved the fit marginally compared with the nonequilibrium model (see simulated BTCs in Figure 4 and r^2 values in Tables 6 and 7). The more complex model predicted the ascending limb and the plateau of the BTC better than the nonequilibrium model but fit the descending limb of the BTC less satisfactorily (Figure 4). Nevertheless, the dual-permeability dual-porosity model yielded physically meaningful θ_{im} and w (fraction of preferential flow porosity) values (Table 7). The θ_{im} values derived from the dual-permeability dual-porosity model (0.08–0.12, with an average of 0.10; Table 7) were less than those derived from the nonequilibrium model but were still significant. The w values (6–11% of the total porosity, average 8%; Table 7) were less than the interpellet porosity (50% of the total porosity), indicating that only a fraction of the interpellet porosity acted as preferential flow paths. The average flux in the matrix was 1.28 cm h^{-1} (Table 7), or 77% of the total flux (1.67 cm h^{-1}). The remaining 23% of the total flux was in the 8% preferential flow porosity, implying that every 1% of the preferential flow porosity carried 2.9% of the total flux.

3.6. Impacts of Preferential Flow and Immobile Water on Contaminant Reduction

[28] The predicted relationships between steady state PCE breakthrough concentration and fraction of preferential flow porosity (w) are depicted in Figure 5. For a θ_{im} of 0.001, the steady state C/C_o increased linearly from 0.0072 to 0.71 (2 orders of magnitude) as the w values increased from 1% to 30% (Figure 5). It is worth noting that the steady state C/C_o increased by almost tenfold (from 0.0072 to 0.070) as w increased from 1% to 5%, demonstrating that

Table 6. Optimized Parameter Values for the Solute Tracers Using the Physical Nonequilibrium Model[a]

Column	α_L, cm	θ_{im}	ω, h^{-1}	K_d, L kg^{-1}	r^2
		Tritium			
1	11.2 ± 22.3	0.19 ± 0.01	0.15 ± 1.75	...	0.91
2	6.7 ± 10.3	0.17 ± 0.01	0.13 ± 1.07	...	0.94
3	8.1 ± 6.9	0.14 ± 0.01	0.15 ± 1.25	...	0.95
4	12.3 ± 16.4	0.14 ± 0.01	0.10 ± 1.11	...	0.94
		Bromide			
1	9.8 ± 16.6	0.15 ± 0.01	0.13 ± 1.67	...	0.91
2	7.5 ± 10.9	0.14 ± 0.01	0.08 ± 0.72	...	0.94
3	8.1[b]	0.15 ± 0.01	0.10 ± 0.83	1.30 ± 0.29	0.89
4	12.3[b]	0.15 ± 0.01	0.06 ± 0.36	1.27 ± 0.31	0.86
Average	9.3	0.15	0.11	1.29	

[a]The 95% confidence limits are indicated by the number following the plus/minus sign.
[b]Fixed and not included in the average.

Table 7. Optimized Parameter Values for the Nonreactive Solute Tracers Using the Dual-Permeability Dual-Porosity Model[a]

Column	q_m, cm h^{-1}	w ($=\theta_f/\theta$)	θ_{im}	α_s ($\times 10^{-4}$ h^{-1})	ω ($\times 10^{-3}$ h^{-1})	$\alpha_{L,f}$, cm	r^2
			Tritium				
1	1.27 ± 0.16	0.06 ± 0.04	0.10 ± 0.10	2.7 ± 5.0	5.2 ± 13.1	1.9 ± 70	0.93
2	1.29 ± 0.07	0.11 ± 0.07	0.11 ± 0.07	1.2 ± 3.5	3.3 ± 5.0	13 ± 30	0.95
3	1.28 ± 0.09	0.09 ± 0.07	0.11 ± 0.03	1.0 ± 1.0	2.3 ± 2.9	2.8 ± 8	0.96
4	1.25 ± 0.16	0.07 ± 0.04	0.08 ± 0.07	3.1 ± 3.7	2.2 ± 4.7	1.9 ± 36	0.95
			Bromide				
1	1.34 ± 0.21	0.08 ± 0.10	0.12 ± 0.10	1.4 ± 2.9	5.0 ± 9.7	4.6 ± 40	0.94
2	1.27 ± 0.12	0.07 ± 0.04	0.10 ± 0.07	5.0 ± 3.7	3.9 ± 7.4	5.8 ± 19	0.95
Average	1.28	0.08	0.10	2.4	3.7	5.0	

[a]The 95% confidence limits are indicated by the number following the plus/minus sign.

even a small preferential flow porosity (e.g., 5%) would drastically lower contaminant removal efficiency (inversely related to the steady state breakthrough concentration). It appears that PCE removal efficiency would not be sensitive to θ_{im} under the transport conditions examined here, as only minor changes in C/C_o are predicted as θ_{im} increased from 0.001 to 0.2 (Figure 5). The minimal impact of θ_{im} on PCE removal efficiency may be due to the relative fast mass transfer between the mobile and immobile regions of the matrix (i.e., $\omega = 3.7 \times 10^{-3}$ h^{-1}).

[29] Linear relationships between steady state PCE breakthrough concentration and immobile water content (θ_{im}) were also predicted (Figure 6). The slope of steady state C/C_o vs. θ_{im} (~0.10, Figure 6) was much less than the slope of C/C_o versus w (~2.5, Figure 5), indicating a much lower dependence of contaminant removal efficiency on θ_{im} than on w under the transport conditions examined. As θ_{im} increased from 0.01 (insignificant immobile water content) to 0.1 (as observed in the SMZ/ZVI pellets used here), the steady state PCE breakthrough concentration (C/C_o) increased from 0.0072 to 0.0115 at $w = 0.001$ and from 0.205 to 0.211 at $w = 0.1$. Such minor increases in C/C_o due to the presence of immobile water (as a result of using fine-grained reactive materials) would be easily compensated by the gain in surface areas and reduction rates (e.g., a tenfold decrease in particle diameter would lead to a 100-fold increase in surface area). Therefore it would still be advantageous to use fine-grained materials in reactive pellets. However, efforts should be made to minimize preferential flow porosity (as observed in pilot- and field-scale PRBs with pelletized reactive materials [*Zhang et al.*, 2001a, 2003] by manufacturing smaller pellets or other means, since even a small fraction of preferential flow porosity may significantly decrease contaminant removal efficiency.

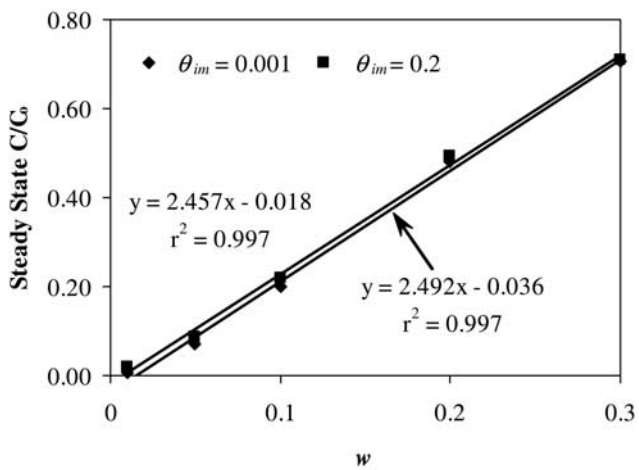

Figure 5. Predicted relationships between steady state perchloroethylene (PCE) breakthrough concentration (C/C_o) and fraction of preferential flow porosity (w). Straight lines are best linear fits. Parameter values used in the dual-permeability and dual-porosity model are $L = 30$ cm, $\theta = 0.81$, $\rho_b = 0.67$ g cm^{-3}, $d = 0.4$ cm, $v = 0.5$ m h^{-1}, $\alpha_{L,m} = 1$ cm, $\alpha_{L,f} = 5$ cm, $\alpha_s = 2.4 \times 10^{-4}$ h^{-1}, $\omega = 3.7 \times 10^{-3}$ h^{-1}, $K_d = 1.0$ L kg^{-1}, and $\mu_s = 0.5$ h^{-1}.

4. Summary and Conclusions

[30] The hydraulic properties of a foamed zeolite/ZVI pellet material were studied by conducting solute and colloidal tracer tests. Preferential flow paths existed between the pellets, as indicated by the enhanced transport of

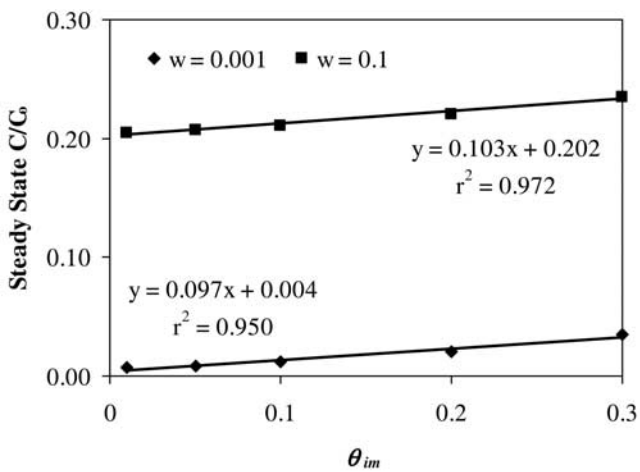

Figure 6. Predicted relationships between steady state PCE breakthrough concentration (C/C_o) and immobile water content (θ_{im}). Straight lines are best linear fits. Parameter values used in the dual-permeability dual-porosity model are the same as in Figure 5.

microspheres relative to tritium and the considerable preferential flow porosity determined by fitting the dual-permeability dual-porosity model. Nonadvective zones existed inside the pellets, as indicated by the rebound of solute concentration during flow interruption and the significant amount of immobile water content determined by fitting the nonequilibrium and dual-permeability dual-porosity models. Quantitatively, the packed pellets had a total porosity of 0.81, of which 50% was large interpellet porosity (0.41) and the remaining was small intrapellet porosity (0.40). About 12–22% of the large interpellet porosity was preferential flow porosity, and about 19–28% of the small intrapellet porosity contained immobile water (based on the dual-permeability dual-porosity model). Forward modeling with the dual-permeability dual-porosity model indicated that the immobile water in the pellets would not significantly affect contaminant removal efficiency. In contrast, the preferential flow porosity would drastically lower contaminant removal efficiency.

Notation

C concentration in aqueous phase, M L^{-3}.
C_o input concentration, M L^{-3}.
C_f solute concentration in fractures, M L^{-3}.
C_m solute concentration in mobile regions of matrix, M L^{-3}.
C_{im} solute concentration in immobile regions of matrix, M L^{-3}.
d effective "diffusion" path length (half the aggregate width or half the fracture spacing), L.
D dispersion coefficient, L^2 T^{-1}.
D_a effective diffusion coefficient, L^2 T^{-1}.
D_f dispersion coefficient in fractures, L^2 T^{-1}.
D_m dispersion coefficient in mobile regions of matrix, L^2 T^{-1}.
e fraction of sorption sites associated with mobile water in matrix.
f fraction of sorption sites associated with fractures.
k_a colloid attachment rate coefficient, T^{-1}.
k_d colloid detachment rate coefficient, T^{-1}.
K_d sorption constant, L^3 M^{-1}.
L column length, L.
q_f flux in fractures, L T^{-1}.
q_m flux in mobile regions of matrix, L T^{-1}.
S concentration on solid phase, M L^{-3}.
t time, T.
v pore water velocity, L T^{-1}.
w ratio of fracture domain to total soil volume.
x travel distance, L.
α_L dispersivity, L.
$\alpha_{L,f}$ dispersivity in fractures, L.
$\alpha_{L,m}$ dispersivity in mobile regions of matrix, L.
α_s first-order solute mass transfer coefficient between fractures and mobile water in matrix, T^{-1}.
β shape factor.
μ_s solid phase first-order decay constant, T^{-1}.
θ total porosity, L^3 L^{-3}.
θ_f fracture (preferential flow) porosity, L^3 L^{-3}.
θ_m porosity in mobile regions of matrix, or porosity accessible to colloids, L^3 L^{-3}.
θ_{im} porosity in immobile regions of matrix, L^3 L^{-3}.
ρ_b bulk density, M L^{-3}.
ω mass transfer coefficient between mobile and immobile water in matrix, T^{-1}.
Γ_s solute mass transfer rate between fractures and mobile water in matrix, M L^{-3} T^{-1}.

[31] **Acknowledgments.** Funding for this research was provided by the U.S. Department of Energy's National Energy Technology Laboratory under contract DE-AR21-95MC32108. The zeolite/ZVI pellets were prepared by Douglas Wolf of the University of Dayton Research Institute. Xian Tao assisted in sample collection and analysis.

References

Bowman, R. S., P. Zhang, X. Tao, R. L. Johnson, and D. Wolf (2002), Surface-altered zeolites as permeable barriers for in situ treatment of contaminated groundwater, Phase IIB topical report to the U.S. Dep. of Energy, Pittsburgh, Pa.

Brusseau, M. L., P. S. C. Rao, R. E. Jessup, and J. M. Davidson (1989), Flow interruption: A method for investigating sorption nonequilibrium, *J. Contam. Hydrol.*, *4*(3), 223–240.

Brusseau, M. L., Q. Hu, and R. Srivastava (1997), Using flow interruption to identity factors causing nonideal contaminant transport, *J. Contam. Hydrol.*, *24*(3–4), 205.

Cao, J., L. Wei, Q. Huang, L. Wang, and S. Han (1999), Reducing degradation of azo dye by zero-valent iron in aqueous solution, *Chemosphere*, *38*(3), 565–571.

Casey, F. X. M., R. Horton, S. D. Logsdon, and D. B. Jaynes (1997), Immobile water content and mass exchange coefficient of a field soil, *Soil Sci. Soc. Am. J.*, *61*(4), 1030–1036.

Champ, D. R., and J. Shroeter (1988), Bacterial transport in fractured rock—A field scale tracer test at the Chalk River Nuclear Laboratories, *Water Sci. Technol.*, *20*(11–12), 81–87.

Deborde, D. C., W. W. Woessner, Q. T. Kiley, and P. Ball (1999), Rapid transport of viruses in a floodplain aquifer, *Water Res.*, *33*(10), 2229–2238.

DeFlaun, M. F., M. E. Fuller, P. Zhang, W. P. Johnson, B. J. Mailloux, W. E. Holben, W. P. Kovacik, D. L. Balkwill, and T. C. Onstott (2001), Comparison of methods for monitoring bacterial transport in the subsurface, *J. Microbiol. Methods*, *47*(2), 219–231.

Freeze, R. A., and J. A. Cherry (1979), *Groundwater*, Prentice-Hall, Upper Saddle River, N. J.

Fuller, M. E., S. H. Streger, R. K. Rothmel, B. J. Mailloux, J. A. Hall, T. C. Onstott, J. K. Fredrickson, D. L. Balkwill, and M. F. DeFlaun (2000), Development of a vital fluorescent staining method for monitoring bacterial transport in subsurface environments, *Appl. Environ. Microbiol.*, *66*(10), 4486–4496.

Gerke, H. H., and M. T. van Genuchten (1996), Macroscopic representation of structural geometry for simulating water and solute movement in dual-porosity flow models, *Adv. Water Resour.*, *29*, 1225–1238.

Gillham, R. W., K. Ritter, Y. Zhang, and M. S. Odziemkowski (2002), Factors in the long-term performance of granular iron PRBs, *IAHS Publ.*, *275*, 421–426.

Ginn, T. R. (2002), A travel time approach to exclusion on transport in porous media, *Water Resour. Res.*, *38*(4), 1041, doi:10.1029/2001WR000865.

Gotpagar, J., E. Grulke, T. Tsang, and D. Bhattacharyya (1997), Reductive dehalogenation of trichloroethylene using zero-valent iron, *Environ. Prog.*, *16*(2), 137–143.

Grant, D. C., M. C. Skriba, and A. K. Saha (1987), Removal of radioactive contaminants from West Valley waste streams using natural zeolite, *Environ. Prog.*, *6*(2), 104–109.

Grolimund, D., M. Elimelech, M. Borkovec, K. Barmettler, R. Kretzschmar, and H. Sticher (1998), Transport of in situ mobilized colloidal particles in packed soil columns, *Environ. Sci. Technol.*, *32*(22), 3562–3569.

Harter, T., S. Wagner, and E. R. Atwill (2000), Colloid transport and filtration of Cryptosporidium parvum in sandy soils and aquifer sediments, *Environ. Sci. Technol.*, *34*(1), 62–70.

Harvey, R. W., and S. P. Garabedian (1991), Use of colloid filtration theory in modeling movement of bacteria through a contaminated sandy aquifer, *Environ. Sci. Technol.*, *25*(1), 178–185.

Harvey, R. W., L. H. George, R. L. Smith, and D. R. LeBlanc (1989), Transport of microspheres and indigenous bacteria through a sandy aquifer: Results of natural- and forced-gradient tracer experiments, *Environ. Sci. Technol.*, *23*(1), 51–56.

Hendry, M. J., J. R. Lawrence, and P. Maloszewski (1997), Role of sorption in the transport of klebsiella oxytoca through saturated silica sand, *Ground Water*, *35*(4), 574–584.

Hendry, M. J., J. R. Lawrence, and P. Maloszewski (1999), Effects of velocity on the transport of two bacteria through saturated sand, *Ground Water*, *37*(1), 103–112.

Hornberger, G. M., A. L. Mills, and J. S. Herman (1992), Bacterial transport in porous media: Evaluation of a model using laboratory observations, *Water Resour. Res.*, *28*(3), 915–938.

Hu, Q., and M. L. Brusseau (1995), Effect of solute size on transport in structured porous media, *Water Resour. Res.*, *31*(7), 1637–1646.

Kjeldsen, P., and T. Locht (2002), Removal of chromate in a permeable reactive barrier using zero-valent iron, *IAHS Publ.*, *275*, 409–414.

Li, Y., and M. Ghodrati (1997), Preferential transport of solute through soil columns containing constructed macropores, *Soil Sci. Soc. Am. J.*, *61*(5), 1308–1317.

Li, Z., and R. S. Bowman (1997), Counterion effects on the sorption of cationic surfactant and chromate on natural clinoptilolite, *Environ. Sci. Technol.*, *31*(8), 2407–2412.

Li, Z., and R. S. Bowman (1998), Sorption of perchloroethylene by surfactant-modified zeolite as controlled by surfactant loading, *Environ. Sci. Technol.*, *32*(15), 2278–2282.

McCaulou, D. R., R. C. Bales, and H. F. McCarthy (1994), Use of short-pulse experiments to study bacteria transport through porous media, *J. Contam. Hydrol.*, *15*(1–2), 1–14.

McKay, L. D., J. A. Cherry, R. C. Bales, M. T. Yahya, and C. P. Gerba (1993), Field example of bacteriophage as tracers of fracture flow, *Environ. Sci. Technol.*, *27*(6), 1075–1079.

Molema, G., G. Mesander, B. Kroesen, W. Helfrich, D. Meijer, and L. de Leij (1998), Analysis of in vitro lymphocyte adhesion and transendothelial migration by fluorescent-beads-based flow cytometric cell counting, *Cytometry*, *32*, 37–43.

Morrison, S. J., D. R. Metzler, and C. E. Carpenter (2001), Uranium precipitation in a permeable reactive barrier by progressive irreversible dissolution of zero-valent iron, *Environ. Sci. Technol.*, *35*(2), 385–390.

Naftz, D. L., C. C. Fuller, J. A. Davis, S. J. Morrison, G. W. Freethey, E. M. Feltcorn, R. G. Wilhelm, M. J. Piana, R. C. Rowland, and J. E. Blue (2000), Field demonstration of permeable reactive barriers to remove dissolved uranium from groundwater, Fry Canyon, Utah, September 1997 through September 1998, *Rep. EPA 402-C-00-001*A, U.S. Environ. Prot. Agency, Washington, D. C.

O'Hannesin, S. F., and R. W. Gillham (1998), Long-term performance of an in situ "iron wall" for remediation of VOCs, *Ground Water*, *36*(1), 164–170.

Pang, L., M. Close, and M. Noonan (1998), Rhodamine WT and bacillus subtilis transport through an alluvial gravel aquifer, *Ground Water*, *36*(1), 112–122.

Ponder, S. M., J. G. Darab, and T. E. Mallouk (2000), Remediation of Cr (VI) and Pb (II) aqueous solutions using supported, nanoscale zero-valent iron, *Environ. Sci. Technol.*, *34*(12), 2564–2569.

Puls, R. W., D. W. Blowes, and R. W. Gillham (1998), Emplacement verification and long-term performance monitoring of a permeable reactive barrier at the USCG Support Center, Elizabeth City, North Carolina, *IAHS Publ.*, *250*, 459–466.

Puls, R. W., D. W. Blowes, and R. W. Gillham (1999a), Long-term performance monitoring for a permeable reactive barrier at the U.S. Coast Guard Support Center, Elizabeth City, North Carolina, *J. Hazard. Mater.*, *68*(1), 109–124.

Puls, R. W., C. J. Paul, and R. M. Powell (1999b), Application of in situ permeable reactive (zero-valent iron) barrier technology for the remediation of chromate-contaminated groundwater: A field test, *Appl. Geochem.*, *14*(8), 989–1000.

Reedy, O. C., P. M. Jardine, G. V. Wilson, and H. M. Selim (1996), Quantifying the diffusive mass transfer of nonreactive solutes in columns of fractured saprolite using flow interruption, *Soil Sci. Soc. Am. J.*, *60*(5), 1376–1384.

Reeter, C., A. Gavaskar, N. Gupta, and B. Sass (1998), Permeable reactive wall remediation of chlorinated hydrocarbons in groundwater, NASA Moffett Field, Mountain View, California, in *Proceedings of the 2nd International Water Resources Engineering Conference, Aug 3–7, 1998*, pp. 153–158, Am. Soc. Civ. Eng., Reston, Va.

Ryan, J. N., and M. Elimelech (1996), Colloid mobilization and transport in groundwater, *Colloids Surf. A*, *107*, 1–56.

Scheibe, T. D., and B. D. Wood (2003), A particle-based model of size or anion exclusion with application to microbial transport in porous media, *Water Resour. Res.*, *39*(4), 1080, doi:10.1029/2001WR001223.

Šimůnek, J., M. Sejna, and M. T. van Genuchten (1998), The HYDRUS-1D software package for simulating the one-dimensional movement of water, heat, and multiple solutes in variably-saturated media, Version 2.0, *Rep. IGWMC-TPS-70*, Int. Ground Water Model. Cent., Colo. School of Mines, Golden, Colo.

Šimůnek, J., N. J. Jarvis, A. Gardenas, and M. T. Van Genuchten (2003), Review and comparison of models for describing non-equilibrium and preferential flow and transport in the vadose zone, *J. Hydrol.*, *272*(1–4), 14–35.

Stewart, C., and J. Steinkamp (1982), Quantification of cell concentration using the flow cytometer, *Cytometry*, *2*, 238–243.

Vilks, P., and D. B. Bachinski (1996), Colloid and suspended particle migration experiments in a granite fracture, *J. Contam. Hydrol.*, *21*(1–4), 269–279.

Vogan, J. L., R. M. Focht, D. K. Clark, and S. L. Graham (1999), Performance evaluation of a permeable reactive barrier for remediation of dissolved chlorinated solvents in groundwater, *J. Hazard. Mater.*, *68*(1), 97–108.

Wang, C.-B., and W.-X. Zhang (1997), Synthesizing nanoscale iron particles for rapid and complete dechlorination of TCE and PCBs, *Environ. Sci. Technol.*, *31*(7), 2154–2156.

Zhang, P., W. P. Johnson, M. J. Piana, C. C. Fuller, and D. L. Naftz (2001a), Potential artifacts in interpretation of differential breakthrough of colloids and dissolved tracers in the context of transport in a zero-valent iron permeable reactive barrier, *Ground Water*, *39*(6), 831–840.

Zhang, P., W. P. Johnson, T. D. Scheibe, K.-H. Choi, F. C. Dobbs, and B. J. Mailloux (2001b), Extended tailing of bacteria following breakthrough at the Narrow Channel focus area, Oyster, Virginia, *Water Resour. Res.*, *37*(11), 2687–2698.

Zhang, P., X. Tao, Z. Li, and R. S. Bowman (2002), Enhanced perchloroethylene reduction in column systems using surfactant-modified zeolite/zero-valent iron pellets, *Environ. Sci. Technol.*, *36*(16), 3597–3603.

Zhang, P., R. S. Bowman, T. L. Johnson, and R. L. Johnson (2003), Influence of preferential flow on perchloroethylene reduction in a surfactant-modified zeolite/zero-valent iron permeable reactive barrier, paper presented at the 2003 Geological Society of America Annual Meeting, Seattle, Wash., 2–5 Nov.

R. S. Bowman, Department of Earth and Environmental Science, New Mexico Institute of Mining and Technology, 801 Leroy Place, Socorro, NM 87801, USA.

J. Šimůnek, Department of Environmental Sciences, University of California, Riverside, 900 University Avenue, Riverside, CA 92521, USA.

P. Zhang, Department of Earth and Atmospheric Sciences, City College of New York, Convent Avenue at 138th Street, New York, NY 10031, USA. (pzhang@sci.ccny.cuny.edu)